



Crystalline carbon nitride semiconductors prepared at different temperatures for photocatalytic hydrogen production

Lihua Lin^{a,b}, Wei Ren^a, Chong Wang^a, A.M. Asiri^c, Jian Zhang^a, Xinchen Wang^{a,*}

^a State Key Laboratory of Photocatalysis on Energy and Environment, College of Chemistry, Fuzhou University, Fuzhou 350116, PR China

^b College of Chemical Engineering, Fuzhou University, Fuzhou 350116, PR China

^c Chemistry Department, Faculty of Science, King Abdulaziz University, Jeddah 21589, Saudi Arabia



ARTICLE INFO

Keywords:

Carbon nitride
Photocatalysis
Crystalline
Heptazine
Hydrogen production

ABSTRACT

Carbon nitride (CN) polymer has been widely investigated as a photocatalyst for solar hydrogen production in recent years due to its unique properties. However, the pristine CN typically shows moderate photocatalytic performance. An important reason is its high-density defects in CN framework, and it could play the role as a recombination center of photogenerated electron-hole pair. Therefore, increasing the crystallinity can be one of efficient way to enhance its photocatalytic activity. Recently, we have report a new heptazine-based crystalline CN synthesized by ionothermal method, and the as-prepared sample has been exhibited high activity toward photocatalytic hydrogen production. Herein, we systematically investigated influences of the synthetic temperature on the properties and photocatalytic activity of the as-prepared crystalline CN polymer. Our results demonstrate that the crystalline CN synthesized by using 550 °C pre-heated precursor shows the highest activity in photocatalytic hydrogen production, and achieving an apparent quantum yield of 6.8%@420 nm with MeOH as sacrificial agent. When compared to the reference photocatalyst P25, the CCN₅₅₀ shows remarkable photocatalytic hydrogen production under visible light irradiation, while P25 is virtually inactive. In addition, the amount of produced hydrogen gas by CCN₅₅₀ is closed to P25 under full arc irradiation of Xe lamp, which highlights the potential solar energy utilization of such crystalline conjugated polymer in the future development.

1. Introduction

As the concerns of globe energy and environmental issues are gradually increasing, much effort has been dedicated to the search of new energy source to replace fossil fuel. Among those, hydrogen gas is a promising clean energy for the future energy supplement due to its high energy density and environmental benign after combustion. In comparison of reforming natural gas, splitting water into hydrogen using sunlight by photocatalyst promises quantities of hydrogen gas as a clean source for energy supply [1–6]. Over the past four decades, significant progress has been made in the development of photocatalysts toward solar water splitting, particularly by conjugated polymers [7–9].

Owing to its uniquely physical and chemical properties, conjugated carbon nitride (CN) polymer has attracted intense interest as photocatalyst since the first discovery of its photocatalytic activity in 2009 [10–13]. However, the pristine CN polymer only shows moderate performance for photocatalytic hydrogen production. One of the important reasons is that the pristine CN polymer that prepared by thermal-induced polymerization typically shows low crystallinity due to the

predominantly kinetic hindrance. The high-density defects in CN frameworks could play the role as recombination center, and leading to a reduced charge carrier transfer efficiency [14,15]. To address this issue, Bojdys et al. used LiCl-KCl as eutectic mixture through high-temperature solution to mediate the polymerization process, and obtained crystalline CN (CCN) polymer [16]. The pioneer work opened up a new avenue to prepare CCN polymer. After that, some CCN polymers have been prepared via ionothermal method [17–20]. The CCN polymer is highly promising in photocatalytic application, because of the fewer defects would reduce the recombination probability and accelerate the transfer of the photogenerated carrier. Besides crystallinity, the type of subunit in CN polymer is another important factor to affect its photocatalytic activity. Generally, the heptazine-based CN polymer would be more favorable for the light harvest and carrier migration than triazine-based CN due to its extended π-conjugated system [21,22]. Unfortunately, the CCN polymer obtained by ionothermal method was mostly constructed by triazine subunit stabilized by the salt residues. Therefore, it is highly desired to synthesize heptazine-based CCN polymer for photocatalytic reactions. Recently, our group has reported

* Corresponding author.

E-mail address: xcwang@fzu.edu.cn (X. Wang).

a heptazine-based CCN semiconductors synthesized by the pre-heated melamine as the heptazine-based precursor and molten salts as high-temperature solution. The as-prepared CCN polymer shows very high photocatalytic activity toward hydrogen production with respect to pristine CN under visible light irradiation [23–25]. Heptazine-based CCN is less studied, but considered as a promising photocatalyst in solar energy utilization. Therefore, it is important to get a deep insight of its properties for further development through optimal synthetic condition. Herein, we systematically study the influence of synthetic temperature on the physicochemical properties and photocatalytic activity of the as-prepared CCN. The sample, which shows the highest photocatalytic activity toward hydrogen production, is synthesized by a calcination of 550 °C pre-heated melamine through molten salt approach. We also compared the as-obtained CCN to the reference photocatalyst P25. The CCN₅₅₀ shows remarkable photocatalytic hydrogen production under visible light irradiation, while P25 is virtually inactive. When the sample is irradiated with full arc of Xe lamp, the amount of produced hydrogen gas by CCN₅₅₀ is closed to P25, which highlights the potential solar energy utilization by such crystalline conjugated polymer in future development.

2. Experimental

2.1. Synthesis of the photocatalysts

Melamine ($C_3H_6N_6$, 99%), KCl (99%) and LiCl (99%) were purchased from Alfa Aesar Chemicals Co. Ltd. (China) and used without further purification. Melamine (8 g) was pre-heated with different temperatures ($T = 450^\circ\text{C}$, 500°C , 550°C and 600°C) for 4 h at a ramping rate of $12^\circ\text{C min}^{-1}$ in a muffle furnace under air atmosphere, the products were referred as bulk CN_T. Then, 600 mg of the pre-heated sample was ground with KCl (3.3 g) and LiCl (2.7 g) in a glove box. Then, the mixture was heated to 550°C for 4 h under N_2 atmosphere (2 L min^{-1}) in a tube furnace. After cooling to the room temperature, the product was washed with boiling deionized water for several times, and product was collected by filtration, followed by drying at 60°C under vacuum. Those samples were denoted as CCN_T, where T indicated the pre-heated temperature.

2.2. Characterization

X-ray diffraction (XRD) measurements were performed on a Bruker D8 Advance diffractometer with Cu-K α 1 radiation ($\lambda = 1.5406\text{ \AA}$). The UV-vis diffuse reflectance spectra (DRS) were performed on a Varian Cary 500 Scan UV-vis system. The Fourier transform infrared (FTIR)

spectra were recorded on a BioRad FTS 6000 spectrometer. The solid-state ^{13}C MAS nuclear magnetic resonance (NMR) spectra were recorded on a Bruker Advance III 500 spectrometer. The photoluminescence (PL) spectra and time-resolved PL were recorded on an Edinburgh FI/FSTCSPC 920 spectrophotometer. The X-ray photoelectron spectroscopy (XPS) data were obtained using a Thermo 6 ESCALAB250 instrument with a monochromatized Al K α line source (200 W). The morphology of the samples was investigated using HITACHI SU8010 field emission scanning electron microscopy (SEM). Transmission electron microscopy (TEM) was performed on a FEI Tenca 20 microscope. Element analysis was carried out on Vario EL Cube. The nitrogen adsorption-desorption isotherms were collected at 77 K using a Micromeritics ASAP 2460 surface area and porosity analyzer. Photocurrent response was performed on BioLogic VSP-300 electrochemical system.

2.3. Photocatalytic reaction

The reactions were carried out in a Pyrex top-irradiation reaction vessel connected to a glass closed gas system. Hydrogen production was performed by dispersing 50 mg of the powder catalyst in an aqueous solution (100 mL) containing 10 mL of methanol (MeOH) as electron donor. Pt (3 wt%) was loaded on the surface of the photocatalyst as a co-catalyst using an in-situ photodeposition method with H_2PtCl_6 as precursor. The reaction solution was evacuated for several times to remove air prior to the irradiation using a 300 W Xe lamp. The wavelength of the incident light was controlled by applying appropriate long-pass cut-off filters. The temperature of the reaction solution was maintained at room temperature using a flow of cooling water during the reaction. The evolved gases were analyzed by a gas chromatography equipped with a thermal conductive detector (TCD) and a 5A molecular sieve column, using argon as the carrier gas. The apparent quantum yield (AQY) for the H_2 evolution was determined by replacing the Xe lamp with a LED equipped with a band-pass filter. The irradiation area was 9 cm^2 and the averaged irradiation intensity of the 420 nm monochromatic light was 7.1 mW cm^{-2} (Newport 2936-R optical power meter). The AQY was calculated as follow:

$$\text{AQY} = N_e/N_p \times 100\% = 2M/N_p \times 100\%$$

where N_e represents the amount of reaction electrons, N_p represents the incident photons and M is the amount of H_2 molecules.

3. Results and discussion

Figs. 1a and S1 show the X-ray diffraction (XRD) of CCN_T and bulk

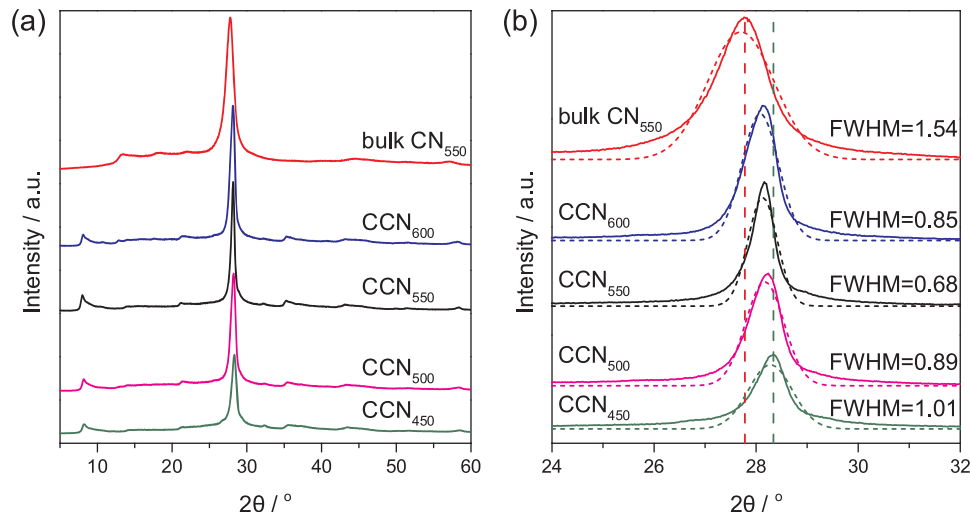


Fig. 1. (a and b) XRD patterns of bulk CN₅₅₀ and CCN_T.

CN_T . For bulk CN_T , phase transition was observed, when the pre-heated temperature was higher than 500 °C as the formation of CN framework [10]. After that, only the peak width and intensity were slightly varied with an increased calcined temperature. For bulk CN_{550} , the strongest peak is located at 27.8°, which can be attributed to the layered stacking of heptazine frameworks. The peak around 13.1° is assigned to the in-plane periodicity [26]. In the case of CCN_T , the strongest peak is slightly shifted to a higher angle than bulk CN_{550} , this phenomenon indicates the decreased interlayer distance due to the enhanced interaction among the layers. A weak peak is observed around 8.1° from CCN_T , corresponding to 1.10 nm of the interplanar distance, which can be attributed to the enlarged in-plane periodicity [27]. As shown in Fig. 1b, the strongest peak in CCN_T shifts to a lower angle as the pre-heated temperature increased, and this result is probably due to the thermal disturbance on the layered structure at a high pre-heated temperature, which leads to the increased interlayer distance. It is worth noting the fact that after heating in molten salts environment, the layered structure is reserved. However, the in-plane periodicity is obviously distinct from the bulk counterpart, indicating the reconstruction of the in-plane structure. Indeed, the C/N mole ratio is increased from 0.647 to 0.683 according to the element analysis (Table S1), which is resulted by the further leaving of amino group and thus achieved the polymerization with higher degree. The full width at half maximum (FWHM) of the strongest diffraction peak in CCN_T is significantly narrowed than bulk CN_{550} , and this observation suggests the improved crystallinity of CCN_T . In addition, the FWHM is decreased with the increased temperature up to 550 °C, beyond which the value is increased, indicating highest crystallinity of CCN_{550} among those samples. To rule out the preferential orientation effects, we have also carried out the XRD with sample spinner, where the samples can rotate around the axis perpendicular to the sample surface. Fig. S2 shows the XRD patterns of CCN_{550} with the spin stage, one can see that under the rotary condition, the peak width of CCN_{550} shows negligible change. Therefore, the narrowed FWHM confirms the better crystallization of CCN_T .

Typical FTIR spectra of bulk CN_T and CCN_T are displayed in Figs. 2a and S3, respectively. The spectrum of bulk CN_T was similar to each other except for bulk CN_{450} , since which was constructed by polymeric melem. The overall patterns of CCN_T are similar to that of bulk CN_{550} , indicating the application of ionothermal method doesn't change the core structure of the CN framework. Severally intense bands are observed at 1200–1700 cm^{-1} , and they are attributed to the stretching modes of the heptazine ring. A sharp peak located at 810 cm^{-1} can be assigned to the characteristic heptazine bending mode [28]. Broad bands are recorded between 3000 and 3500 cm^{-1} , and they are originated from the stretching mode of bridged or terminal amino group [29]. Furthermore, those results also demonstrated that the pre-heated temperature cannot influence the core chemical structure of CCN_T . However, a striking difference between bulk CN_{550} and CCN_T around 2170 cm^{-1} is due to the stretch of the cyano group, which is resulted from the loss of ammonia [30]. It is most likely due to the partial decomposition of the heptazine rings under high temperature in the molten salt.

The light-harvesting ability of bulk CN_T and CCN_T was measured by UV-vis diffuse reflectance spectra (DRS). As shown in Fig. S4, the absorption intensity of bulk CN_T was gradually increased with the calcined temperature up to 550 °C and decreased in 600 °C. The absorption edge of bulk CN_T shows a same trend, which is probably related to the formation and decomposition of heptazine unit. In Fig. 2b, the CCN_T samples exhibit a typical absorption, and it indicates its intrinsic semiconductor properties. Obviously, the optical absorption strengths of the CCN_T are significant increased with respect to that of the bulk one. According to the literatures, the light-harvesting ability of the conjugated polymer is associated with its structural rigidity [31]. Therefore, the enhanced optical absorption strength of CCN_T can be attributed to the increased chain stiffness with the enhanced interaction between the subunits. In general, a higher optical absorption is critical

to the performances of photocatalysts, because an increased number of incident photons can be utilized in the photocatalytic process. In addition, the absorption intensity is gradually enhanced with the increased pre-heated temperature up to 550 °C, beyond which the absorption intensity is decreased. The absorption edge of CCN_{600} shows slightly blue-shifted among the CCN_T samples, which is probably due to the quantum confinement effect because the higher calcined temperature would split the precursor into small pieces [32]. The light absorption ability was further investigated by photocurrent response test. As shown in Fig. S5, all the CCN_T samples show significantly enhanced photocurrent compared with bulk CN_{550} . The photocurrents of CCN_T were gradually increased with increasing the pre-heated temperature up to 550 °C, and decreased in 600 °C, these observations are consistent with the DRS results.

The photoluminescence (PL) is related to the recombination of photogenerated charge carriers in photocatalysts. The CN polymer possesses delocalized electrons in the conjugated backbone, which formed π^* anti-bonding orbital. Therefore, the PL emission is dominated by the recombination of electron-hole pairs between lone pair valence band and π^* conduction band. In principle, the intensity of the PL peak can be reduced by extending π -conjugated system via connecting more heptazine units which results in an increased π state and stronger orbital overlap [33]. In addition, the PL intensity can also be reduced by decreasing the structure defects which usually plays the role as recombination center [34]. As shown in Fig. 2c, border peaks are centered at around 460 nm, corresponding to the intra-band transition between VB and CB [35]. As expected, the CCN_T samples show significantly decreased fluorescence-strength with respect to the bulk CN_{550} . The lower fluorescence intensity of CCN_T typically indicates the lower electron-hole recombination rate [36]. Therefore, the PL results further confirmed the reduced defects from CCN_T frameworks and the improved electron transfer ability [37]. The CCN_{600} shows the highest PL emission among the CCN_T samples. It is most likely due to the structure distortion of the precursor under the high pre-heated temperature, and the result is consistent with the XRD analysis. In addition, the time-resolved PL experiments in Fig. 2d shows a faster PL decay of all CCN_T samples compared with bulk CN_{550} , while the CCN_T samples exhibit similar decay rate with each other. The weighted mean lifetime of bulk CN_{550} and CCN_{550} obtained by fitting the decay curves are 5.42 ns and 3.61 ns. Since those measurements were performed using powder form, the decreased PL intensity and lifetime are solvent-free effects. It is most likely due to the excited state electron transfer from the bulk to the electron acceptor of cyano group [38]. Such fast electron migration would be favorable for the separation of the photogenerated carriers and enhanced the photocatalytic activity in principle.

The nitrogen adsorption-desorption isotherms were used to investigate the porosity and surface area of bulk CN_{550} and CCN_T . As shown in Fig. 3a, significantly increased surface areas of CCN_T are observed compared with bulk CN_{550} [39]. The BET surface areas are 105, 113, 115, 87 and 15 $\text{m}^2 \cdot \text{g}^{-1}$ for CCN_{450} , CCN_{500} , CCN_{550} , CCN_{600} and bulk CN_{550} , respectively. These results indicate the pre-heated temperatures have less influence on the surface area up to 500 °C. However, the surface area decreased with pre-heated temperature of 600 °C. It may due to that the high temperature would split the precursor into small nanoparticles, which would fill the void of the stacked pores. As shown in Fig. 3b, the pore size distributions determined by the BJH desorption method indicate the mean pore sizes are centered at approximately 12–14 nm for CCN_T , and this result is owing to the stacked pore of the nanoparticles.

The morphologies of bulk CN_{550} and CCN_T were investigated by field emission scanning electron microscopy (SEM). In Fig. 4a, the SEM image of the bulk CN_{550} synthesized by traditional thermal-induced polycondensation typically shows stacking of bulk particles [40]. In contrast, the CCN_T shows large-scale regular nanorods with stacking pore structure, as shown in Fig. 4b–e. It is notable that the CN became longer and thicker with the increased pre-heated temperature. When

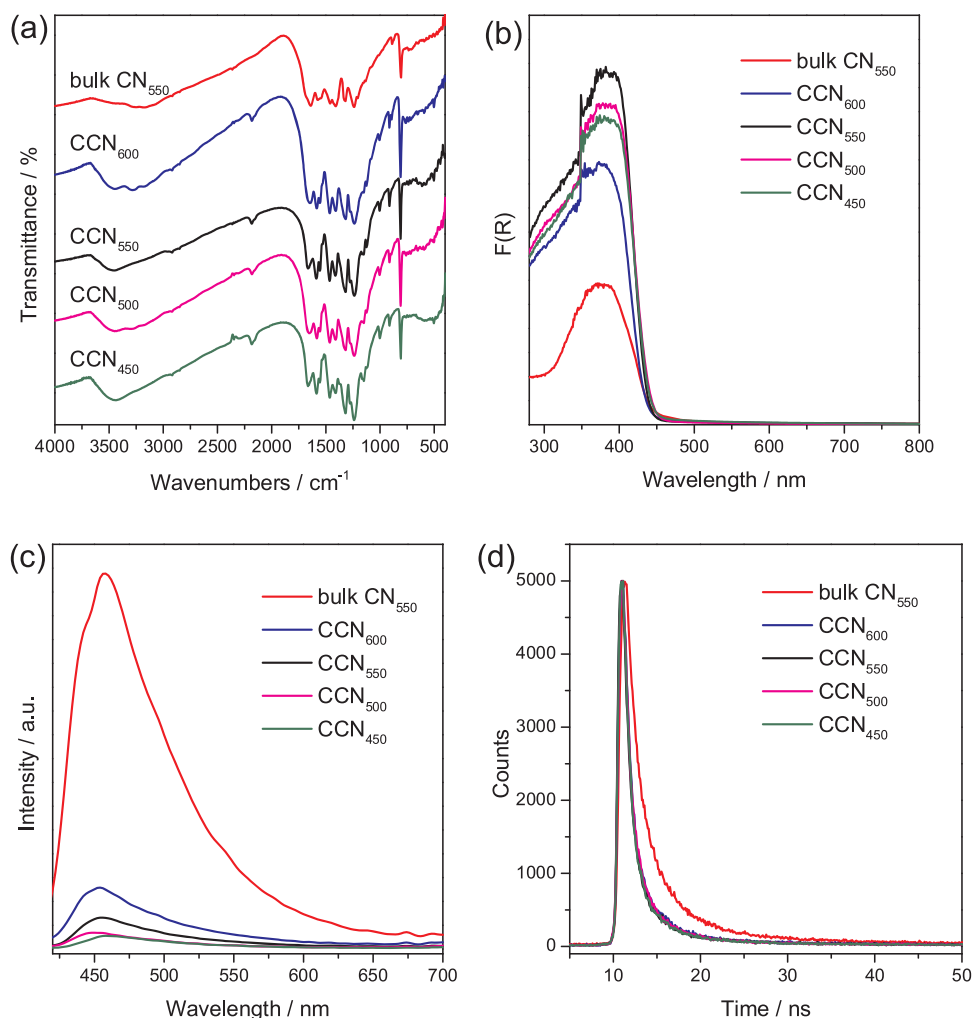


Fig. 2. (a) FT-IR spectra and (b) UV-vis DRS of bulk CN₅₅₀ and CCN_T. (c) PL spectra of the bulk CN₅₅₀ and CCN_T. (d) Time-resolved PL spectra of bulk CN₅₅₀ and CCN_T under 408 nm laser excitation.

the temperature was increased to 600 °C, dense nanoparticles appeared instead of the nanoroads, which is owing to the decomposed of the precursor into nanoparticles at high pre-heated temperature. In addition, using molten salts shows more “green” approach to control the morphology compared with soft/hard-template methods, in which the toxic ammonium bifluoride or hydrofluoric acid is typically used to

remove the silicon template [41,42]. On the contrary, the salts can simply remove by washing with water. The improved crystallinity of CCN_T was further confirmed by high-resolution TEM analysis, as shown in Fig. 4f. A clear lattice fingers are observed in CCN₅₅₀ and the d-space of the lattice finger is measured as 0.32 nm, which is in consistent with the XRD results.

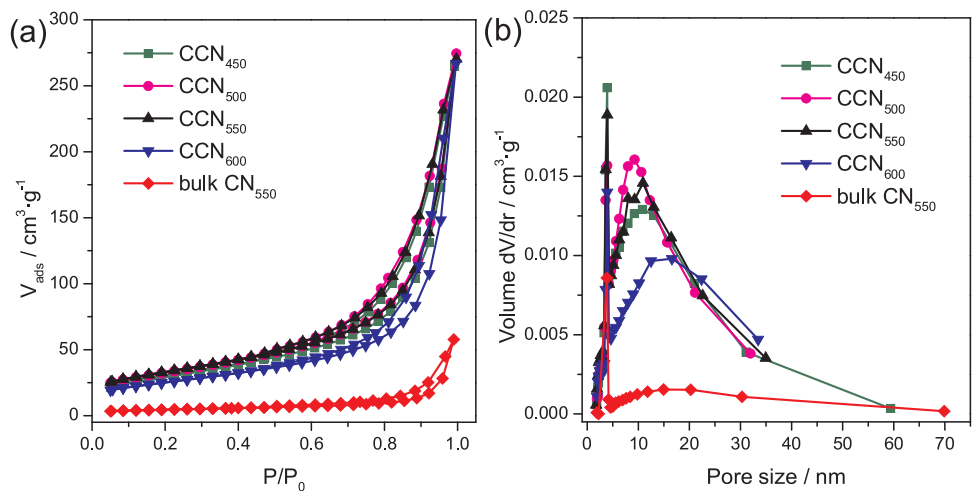


Fig. 3. (a) N₂-sorption isotherms collected at 77 K and (b) pore size distribution of the samples.

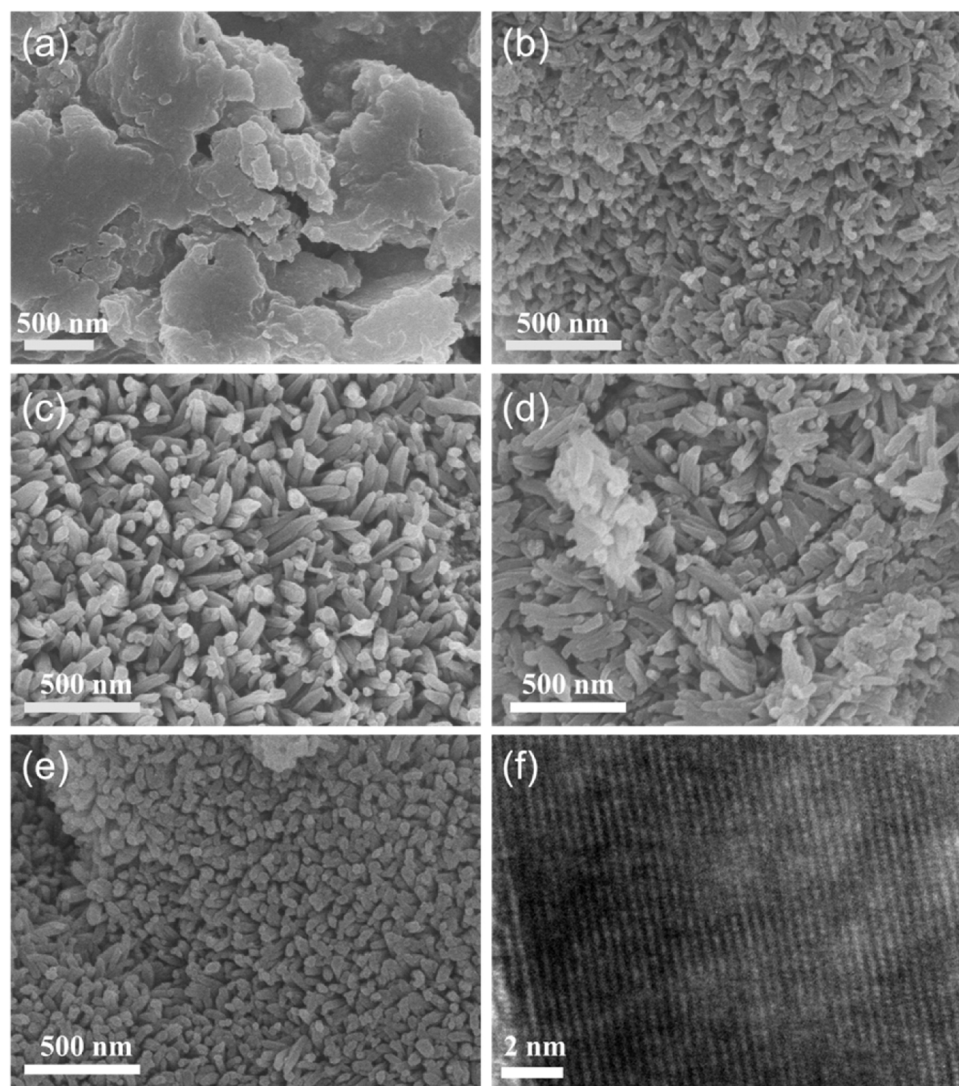


Fig. 4. SEM images of (a) bulk CN₅₅₀, (b) CCN₄₅₀, (c) CCN₅₀₀, (d) CCN₅₅₀, (e) CCN₆₀₀. (f) TEM image of the CCN₅₅₀.

Figs. 5 and S6 show the X-ray photoelectron spectroscopy (XPS) of bulk CN₅₅₀ and CCN_T, respectively. There are three elements (C, N, and O) in the survey spectrum of bulk CN₅₅₀. The high resolution of C 1s spectrum is deconvoluted into two peaks at 288.1 eV and 284.8 eV. The former intense peak is attributed to the sp²-hybridized of graphitic carbon atoms in N-contained heptazine rings (N—C=N), while the latter one is probably originated from the adventitious carbon (such as grease) [43,44]. The N 1s can be decomposed into four peaks. The peak located at 398.6 eV is assigned to the pyridine-like N involved in the heptazine rings (C—N=C). The peak at 399.9 eV can be assigned to the bridged or terminal amino groups, while the 401.8 eV is attributed to the central N atoms of heptazine rings in the form of “graphitic” nitrogen [45]. The small peak at 404.8 eV is typical assigned to the charging effects or positive charge localization in heterocycles. In the case of CCN₅₅₀, the C 1s spectrum is deconvoluted into three peaks. The peak located at 288.5 eV is attributed to the sp²-bonds of N—C=N. The weak peak at 286.4 eV is probably originated from cyano group. Four peaks are found in N 1s spectrum. Similar to bulk CN₅₅₀, the peaks located at 398.9 and 401.8 eV are assigned to heptazine rings (C—N=C) and N—(C)₃, respectively, whereas the peaks at 400.6 eV is assigned to the bridged or terminal amino groups. Owing to the overlap of cyano group and amino group, the peak of cyano group is not fitted in N 1s spectrum [46]. An additional K 2p peaks are observed in CCN₅₅₀, and this result may induced from the surface bonded or layered intercalated

K ions [47]. The K⁺ was mostly likely acted as the charge compensator due to the loss of hydrogen in the form of NH₃ during the treatment in molten salts (Fig. S7). In addition, the incorporated of K⁺ in CN framework may increase the conductivity, which would be favorable for the carrier transfer. It is worth noting that the peak positions of the CCN_T are nearly same between each other, indicating the pre-heated temperature has less influence on the chemical state of those samples. In addition, O atoms signal is detected in both bulk CN₅₅₀ and CCN₅₅₀. We assumed that the oxygen signals are originated from the absorbed O₂ or H₂O molecules [48]. This conclusion was confirmed by the XPS with surface Ar⁺ etching, as shown in Fig. 5h, the signal of O 1s is significantly decreased after 30 s etch.

To investigate the subunits of the CCN_T, we have carried out the NMR experiments. It is well known that there are two based subunits in carbon nitride frameworks, i.e., triazine and heptazine [49]. Previous works have demonstrated that carbon atoms in triazine units induce the NMR peak around 164 ppm, corresponding to the C(e) (N—C=N). While in the case of the heptazine units, there are two carbon atoms peaks appearing in the NMR spectrum. One of the peaks is similar to the triazine unit and the other is located at about 155 ppm, corresponding to C(i) (C—N₃) [50–52]. Therefore, the NMR technique is a powerful tool to distinguish the subunit of the carbon nitride framework. In Fig. 6, two sharp peaks are located at 163 ppm and 157 ppm with approximate equivalent peak area, and these results confirms the present

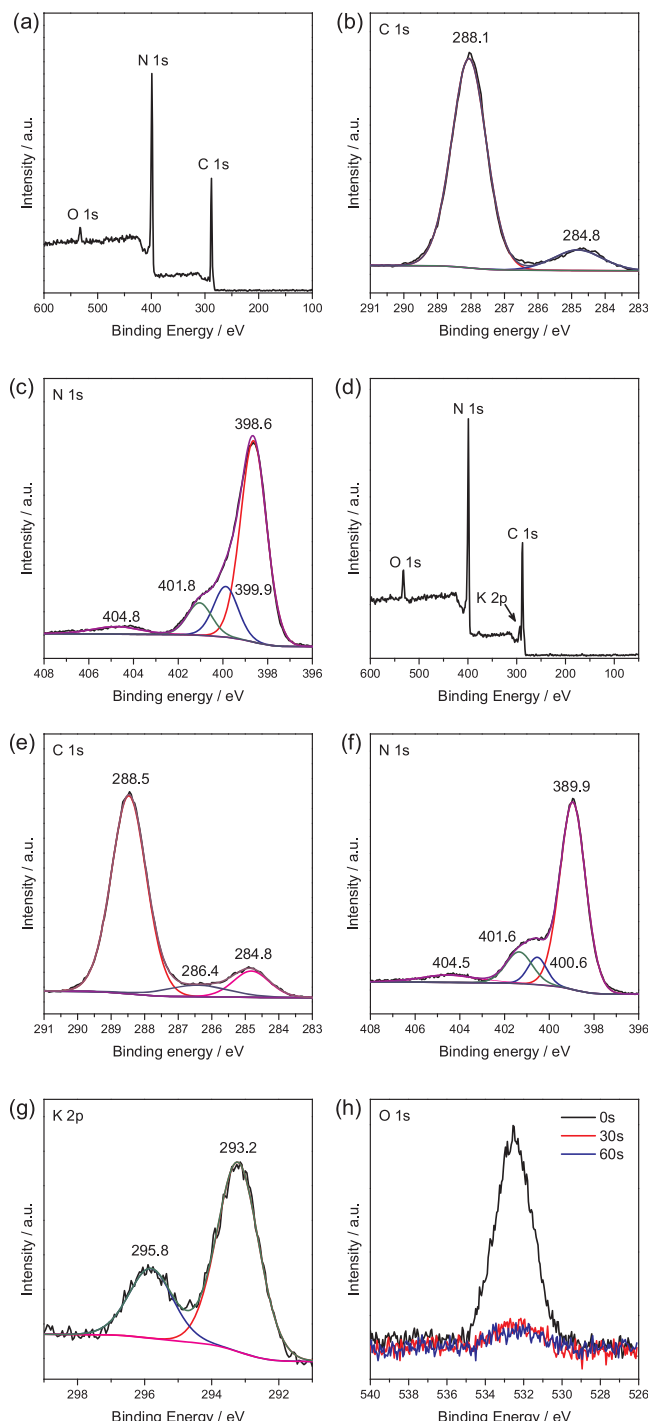


Fig. 5. (a) XPS of bulk CN₅₅₀ and the corresponding (b) C 1s and (c) N 1s. (d) XPS of CCN₅₅₀ and the corresponding (e) C 1s, (f) N 1s and (g) K 2p. (h) O 1s spectrum of CCN₅₅₀ using surface Ar⁺ etching.

of the heptazine subunits in CCN₅₅₀ framework. In addition, the using of ionothermal method is mostly formed triazine-based CCN in previous literatures, such as PTI/Li⁺Cl⁻ [53]. Therefore, our work provides a new method to synthesize CCN with heptazine motifs. In principle, the heptazine-based CN would be more favorable for the light-harvesting and accelerating the migration of the photogenerated electron due to the extending π -conjugated system.

Photocatalytic hydrogen production was carried out in methanol/water (1:10 vol%) solution and 3 wt% Pt was loaded on the photocatalyst surface as the co-catalyst by using photo-deposition method

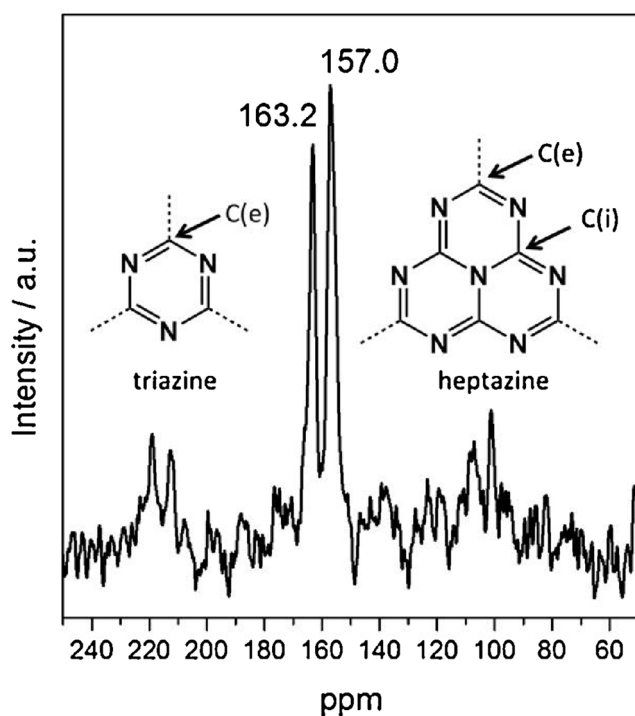


Fig. 6. ^{13}C direct excitation spectrum of CCN₅₅₀.

using H₂PtCl₆ as precursor. As shown in Fig. 7a, the hydrogen evolution rate (HER) is gradually increased with the increased pre-heated temperature and reaches the maximum value at 550 °C. After that, the HER is decreased with the increased pre-heated temperature, which is probably due to the decrease in the light-harvesting ability and surface area. Among the CCN_T samples, HER using CCN₅₅₀ is highest reaching to 33 $\mu\text{mol h}^{-1}$ under > 420 nm light irradiation. The weight-dependent HER was also performed. In Fig. 7b, the optimal weight of photocatalyst of CCN₅₅₀ is 100 mg under the present reaction conditions. HER is decreased when further increased the amount of photocatalyst and finally reached an equilibrium. This is because of the high concentrated photocatalyst would shield the incident light and only those photocatalyst near the water surface can functionalized to absorb light. We also studied the influence of the Pt content toward the photocatalytic activity. The loading of Pt can effectively lower the overpotential of water reduction, and acts as the activity sites on the catalyst surface. As shown in Fig. 7c, the HER is significantly enhanced by increasing Pt content from 2 wt% to 3 wt%. However, further increasing Pt content to 4 wt% leads to the decreased HER. This is probably due to that the over-loaded Pt would block the incident light. The photocatalytic activity of CCN₅₅₀ was also compared to that of the reference photocatalyst P25 (commercial TiO₂) under the same experimental conditions. Fig. S8 shows the comparison of CCN₅₅₀ and P25 under full arc irradiation of Xe lamp. The produced H₂ increases steadily with prolonged time of the light irradiation, and the results demonstrate that CCN₅₅₀ can photocatalyze 2.24 mmol H₂ in 4 h, while it is 3.02 mmol by P25. Note that P25 is virtually inactive under visible light irradiation. However, the CCN₅₅₀ shows remarkable photocatalytic hydrogen production activity, as shown in Fig. 7d. Therefore, those results highly promise such crystalline polymer photocatalyst in sustainable H₂ production with future development.

To further confirm that water reduction is indeed driven by visible absorption by the carbon nitride catalyst, a wavelength dependent H₂ evolution experiment was also carried out by using different monochromatic light. In Fig. 8a, the apparent quantum yield (AQY) values match well with the DRS spectrum. Those results strongly support that the hydrogen production process is primarily driven by light-induced of

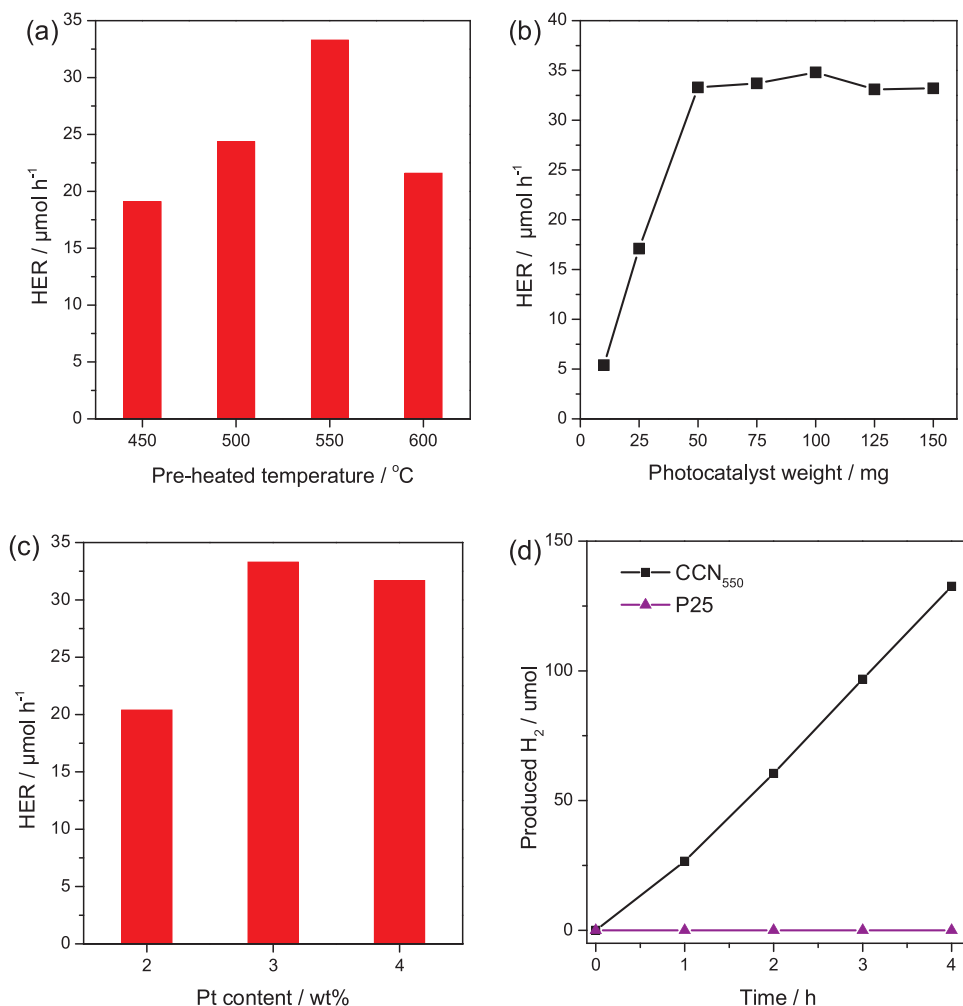


Fig. 7. (a) The HER of CCN_T samples. (b) The weight-dependent HER of CCN_{550} . (c) The HER of CCN_{550} by loading different amount of Pt as the cocatalyst. (d) The hydrogen production of CCN_{550} and P25 under $> 420 \text{ nm}$ light irradiation using MeOH as sacrificial agent.

electrons in the CN polymer. In addition, the AQY was determined as 6.8% by using 420 nm monochromatic light with MeOH as sacrificial agent. Subsequently, we performed the weight-dependent AQY under 420 nm monochromatic light using CCN_{550} as the photocatalyst. As shown in Fig. 8b, the AQY value is gradually increased with the increase of photocatalyst weight, and reached the maximum value using

50 mg. Beyond which, the AQY value is decreased. Those results suggest that the AQY value is directly related to the quantity of the photocatalyst [15]. Similar to the results from weight-dependent experiment, this is because the incident light was directly passed the water at low photocatalyst concentration and cannot be absorbed effectively. On the contrary, only this photocatalyst near the water surface can

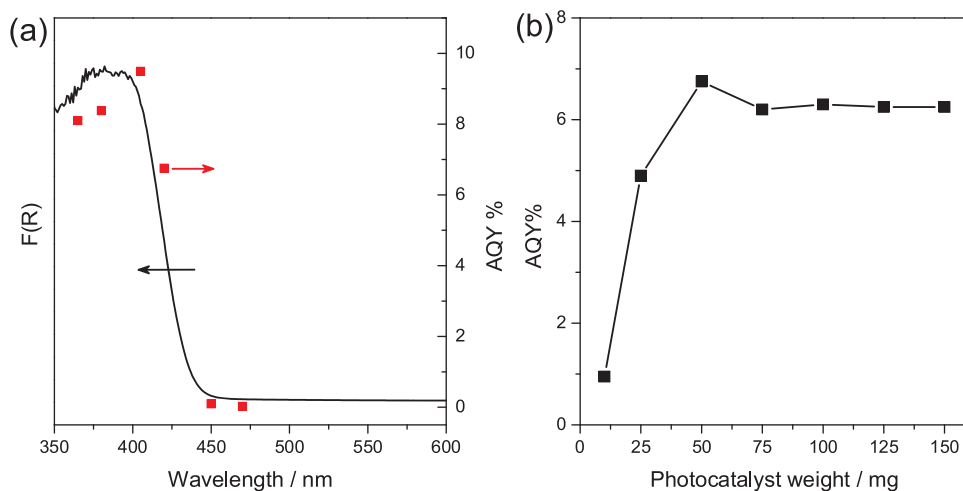


Fig. 8. (a) Wavelength-dependent HER of CCN_{550} . (b) Weight-dependent AQY of CCN_{550} using 420nm monochromatic light irradiation and MeOH as sacrificial agent.

absorbed the light at high concentration. Finally, the H₂ production of CCN₅₅₀ was performed with prolonged time for 24 h. As shown in Fig. S9, no obvious decay was found after 6 consecutive cycles for the photocatalytic reactions, and this result indicates the well stability of CCN₅₅₀.

4. Conclusions

In summary, we have investigated the influence of the pre-heated temperature of melamine on crystalline CN via ionothermal method. Those results show that the crystallinity and light absorption of the samples were enhanced with the increased pre-heated temperature up to 550 °C. Further increasing the pre-heated temperature leads to decrease crystallinity and the light absorption. The recombination rate of photogenerated electron-holes was gradually increased with increased pre-heated temperature, but still significant lower than that of bulk CN₅₅₀. On the contrary, the pre-heated temperature has less influence on core chemical structure and morphology of CCN_T, as reflected by the results of FTIR, NMR, XPS and SEM. Photocatalytic hydrogen production activity shows similar trend as the light absorption ability with the different pre-heated temperature. Due to highest crystallinity and light absorption ability among those samples, together with the lower electron-holes recombination rate, the optimal sample of CCN₅₅₀ shows the highest photocatalytic activity, and it reached 33 μmol h⁻¹ under > 420 nm light irradiation by using MeOH as sacrificial agent, which is 1.7 time higher than CCN₄₅₀. The hydrogen production ability of CCN₅₅₀ was also comparable to reference photocatalyst P25 under full arc irradiation of Xe lamp. Our work provides a path to synthesis heptazine-based crystalline CN with high photocatalytic activity and may extend to other application by solar energy utilization, such as photocatalytic CO₂ reduction and organic photosynthesis.

Acknowledgment

This work was financially supported by the National Natural Science Foundation of China (21425309 and 21761132002) and the 111 Project.

Appendix A. Supplementary data

Supplementary material related to this article can be found, in the online version, at doi:<https://doi.org/10.1016/j.apcatb.2018.03.009>.

References

- [1] A. Fujishima, K. Honda, *Nature* 238 (1972) 37–38.
- [2] S. Chen, T. Takata, K. Domen, *Nat. Rev. Mater.* 2 (2017) 17050.
- [3] N.S. Lewis, *Science* 351 (2016) 353.
- [4] X. Chen, C. Li, M. Gratzel, R. Kostecki, S.S. Mao, *Chem. Soc. Rev.* 41 (2012) 7909–7937.
- [5] Z. Li, W. Luo, M. Zhang, J. Feng, Z. Zou, *Energy Environ. Sci.* 6 (2013) 347–370.
- [6] H. Tong, S. Ouyang, Y. Bi, N. Umezawa, M. Oshikiri, J. Ye, *Adv. Mater.* 24 (2012) 229–251.
- [7] T. Hisatomi, J. Kubota, K. Domen, *Chem. Soc. Rev.* 43 (2014) 7520–7535.
- [8] A. Kudo, Y. Misaki, *Chem. Soc. Rev.* 38 (2009) 253–278.
- [9] R.S. Sprick, J.-X. Jiang, B. Bonillo, S. Ren, T. Ratvijitvech, P. Guiglion, M.A. Zwijnenburg, D.J. Adams, A.I. Cooper, *J. Am. Chem. Soc.* 137 (2015) 3265–3270.
- [10] X. Wang, K. Maeda, A. Thomas, K. Takanabe, G. Xin, J.M. Carlsson, K. Domen, M. Antonietti, *Nat. Mater.* 8 (2009) 76–80.
- [11] Y. Zheng, L. Lin, B. Wang, X. Wang, *Angew. Chem. Int. Ed.* 54 (2015) 12868–12884.
- [12] S. Cao, J. Low, J. Yu, M. Jaroniec, *Adv. Mater.* 27 (2015) 2150–2176.
- [13] W.-J. Ong, L.-L. Tan, Y.H. Ng, S.-T. Yong, S.-P. Chai, *Chem. Rev.* 116 (2016) 7159–7329.
- [14] K. Maeda, *ACS Catal.* 3 (2013) 1486–1503.
- [15] H. Kato, K. Asakura, A. Kudo, *J. Am. Chem. Soc.* 125 (2003) 3082–3089.
- [16] M.J. Bojdys, J.-O. Müller, M. Antonietti, A. Thomas, *Chem. Eur. J.* 14 (2008) 8177–8182.
- [17] Y. Ham, K. Maeda, D. Cha, K. Takanabe, K. Domen, *Chem. Asian J.* 8 (2013) 218–224.
- [18] G. Algara-Siller, N. Severin, S.Y. Chong, T. Björkman, R.G. Palgrave, A. Laybourn, M. Antonietti, Y.Z. Khimyak, A.V. Krasheninnikov, J.P. Rabe, U. Kaiser, A.I. Cooper, A. Thomas, M.J. Bojdys, *Angew. Chem. Int. Ed.* 53 (2014) 7450–7455.
- [19] M.K. Bhunia, K. Yamauchi, K. Takanabe, *Angew. Chem. Int. Ed.* 53 (2014) 11001–11005.
- [20] D. Dontsova, C. Fettkenhauer, V. Papaefthimiou, J. Schmidt, M. Antonietti, *Chem. Mater.* 28 (2016) 772–778.
- [21] D. Kim, A. Osuka, *Acc. Chem. Res.* 37 (2004) 735–745.
- [22] G. Li, W.-H. Chang, Y. Yang, *Nat. Rev. Mater.* 2 (2017) 17043.
- [23] L. Lin, H. Ou, Y. Zhang, X. Wang, *ACS Catal.* 6 (2016) 3921–3931.
- [24] H. Ou, L. Lin, Y. Zheng, P. Yang, Y. Fang, X. Wang, *Adv. Mater.* 29 (2017) 1700008.
- [25] G. Zhang, G. Li, Z.-A. Lan, L. Lin, A. Savateev, T. Heil, S. Zafeiratos, X. Wang, M. Antonietti, *Angew. Chem. Int. Ed.* 56 (2017) 13445–13449.
- [26] J. Zhang, M. Zhang, G. Zhang, X. Wang, *ACS Catal.* 2 (2012) 940–948.
- [27] B. Kurpil, A. Savateev, V. Papaefthimiou, S. Zafeiratos, T. Heil, S. Özenler, D. Dontsova, M. Antonietti, *Appl. Catal. B: Environ.* 217 (2017) 622–628.
- [28] Y. Wu, M. Wen, M. Navlani-García, Y. Kuwahara, K. Mori, H. Yamashita, *Chem. Asian J.* 12 (2017) 860–867.
- [29] A.B. Jorge, D.J. Martin, M.T.S. Dhanoa, A.S. Rahman, N. Makwana, J. Tang, A. Sella, F. Corà, S. Firth, J.A. Darr, P.F. McMillan, *J. Phys. Chem. C* 117 (2013) 7178–7185.
- [30] H. Gao, S. Yan, J. Wang, Y.A. Huang, P. Wang, Z. Li, Z. Zou, *Phys. Chem. Chem. Phys.* 15 (2013) 18077–18084.
- [31] M.S. Vezie, S. Few, I. Meager, G. Pieridou, B. Dorling, R.S. Ashraf, A.R. Goni, H. Bronstein, I. McCulloch, S.C. Hayes, M. Campoy-Quiles, J. Nelson, *Nat. Mater.* 15 (2016) 746–753.
- [32] P. Niu, L. Zhang, G. Liu, H.-M. Cheng, *Adv. Funct. Mater.* 22 (2012) 4763–4770.
- [33] Y. Chen, B. Wang, S. Lin, Y. Zhang, X. Wang, *J. Phys. Chem. C* 118 (2014) 29981–29989.
- [34] U. Diebold, *Nat. Chem.* 3 (2011) 271–272.
- [35] M. Zhang, X. Wang, *Energy Environ. Sci.* 7 (2014) 1902–1906.
- [36] Q. Han, B. Wang, Y. Zhao, C. Hu, L. Qu, *Angew. Chem.* 54 (2015) 11433–11437.
- [37] Z.-A. Lan, G. Zhang, X. Wang, *Appl. Catal. B* 192 (2016) 116–125.
- [38] M.Y. Berezin, S. Achilefu, *Chem. Rev.* 110 (2010) 2641–2684.
- [39] F. Dai, J. Zai, R. Yi, M.L. Gordin, H. Sohn, S. Chen, D. Wang, *Nat. Commun.* 5 (2014) 3605.
- [40] M. Zhang, W. Jiang, D. Liu, J. Wang, Y. Liu, Y. Zhu, Y. Zhu, *Appl. Catal. B: Environ.* 183 (2016) 263–268.
- [41] X. Wang, K. Maeda, X. Chen, K. Takanabe, K. Domen, Y. Hou, X. Fu, M. Antonietti, *J. Am. Chem. Soc.* 131 (2009) 1680–1681.
- [42] Y. Zheng, L. Lin, X. Ye, F. Guo, X. Wang, *Angew. Chem. Int. Ed.* 53 (2014) 11926–11930.
- [43] K. Schwinghammer, M.B. Mesch, V. Duppel, C. Ziegler, J. Senker, B.V. Lotsch, *J. Am. Chem. Soc.* 136 (2014) 1730–1733.
- [44] M. Zhang, Z. Luo, M. Zhou, G. Zhang, K.A. Alamry, L.A. Taib, A.M. Asiri, X. Wang, *Appl. Catal. B* 210 (2017) 454–461.
- [45] Z.-H. Sheng, L. Shao, J.-J. Chen, W.-J. Bao, F.-B. Wang, X.-H. Xia, *ACS Nano* 5 (2011) 4350–4358.
- [46] V.N. Khabashesku, J.L. Zimmerman, J.L. Margrave, *Chem. Mater.* 12 (2000) 3264–3270.
- [47] D. Dontsova, S. Pronkin, M. Wehle, Z. Chen, C. Fettkenhauer, G. Clavel, M. Antonietti, *Chem. Mater.* 27 (2015) 5170–5179.
- [48] G. Zhang, J. Zhang, M. Zhang, X. Wang, J. Mater. Chem. 22 (2012) 8083–8091.
- [49] J.R. Holst, E.G. Gillan, *J. Am. Chem. Soc.* 130 (2008) 7373–7379.
- [50] B. Jürgens, E. Irran, J. Senker, P. Kroll, H. Müller, W. Schnick, *J. Am. Chem. Soc.* 125 (2003) 10288–10300.
- [51] Y. Gui, Z. Ding, X. Fu, X. Wang, *Angew. Chem. Int. Ed.* 51 (2012) 11814–11818.
- [52] B.V. Lotsch, M. Döblinger, J. Sehnert, L. Seyfarth, J. Senker, O. Oeckler, W. Schnick, *Chem. Eur. J.* 13 (2007) 4969–4980.
- [53] L. Lin, C. Wang, W. Ren, H. Ou, Y. Zhang, X. Wang, *Chem. Sci.* 8 (2017) 5506–5511.